Test facility for building envelope leakage type analysis and improvement of acoustic and thermographic airtightness measurement methods

Markus Diel[*1], Björn Schiricke[1], Johannes Pernpeintner[1]

1 German Aerospace Center (DLR e.V.)
Institute of Solar Research
Linder Hoehe
51147 Cologne, Germany
**Corresponding author: markus.diel@dlr.de*

ABSTRACT

Ensuring the airtightness of building envelopes is crucial for enhancing the energy efficiency of buildings. The prompt detection of leaks is essential, particularly when undertaking building renovations. Consequently, efforts have been made in recent years to implement new measurement techniques that facilitate the rapid, straightforward, and wide-scale identification of leaks in building envelopes. Two notable methods are the use of acoustic and thermographic technologies. In the acoustic beamforming method, a microphone array technology is employed, whereby sound propagation is assumed to occur in a manner similar to that of airflow through the building envelope. The infrared camera, however, is capable of rapidly identifying problem areas through the use of intelligent experimental setups.

Although both methodologies have undergone preliminary evaluation on smaller façade elements and in field trials, this paper presents the initial findings of the first large-scale laboratory testing of these methodologies in the context of leak detection on building envelopes. To facilitate the investigation on such a comprehensive level, a new airtightness test facility was constructed. This test facility has a volume of approx. 11.4 m^3, has an n50 value of 0.0088 and can hold test specimens of various sizes up to 3 m^2.

Initial investigations utilising an acoustic camera revealed that a simple leakage in the form of a 3.3 mm hole could be precisely localised at different measurement distances. Furthermore, it was demonstrated that the spectra of different hole sizes exhibited a similar curve shape, and that there was a correlation between the maximum sound pressure level and the hole size.

Thermographic measurements with 6-7 K temperature difference, 50 Pa pressure were performed with camera distances between 1.5 m and 5.0 m at normal and 45° angle. Individual leaks of 3.3 mm diameter could be detected at all distances. With lager distance and shallower incidence angle, the signal reduced, but localization was possible with objects smaller than the pixel-resolution.

The outcomes of the tests conducted at the test facility confirmed the assumption that comprehensive laboratory testing is essential for a more accurate evaluation of both methods in the context of leak detection on building envelopes, and thus for subsequent field use. Further measurement campaigns are already underway and will continue to investigate the methods themselves, as well as more complex and therefore more realistic leakages.

KEYWORDS

Airtightness, Acoustic Beam Forming, Thermography, Leak Localization, Test Facility

1 INTRODUCTION

It is estimated that approximately 30% of the energy consumed by a building for the purposes of heating and cooling can be attributed to unwanted air exchange through the building envelope (Jokisalo, Kurnitski, Korpi, Kalamees, & Vinha, 2009; Sawyer, 2014). The main method used

to measure the aggregated airtightness of buildings is the fan pressurisation method or “blower door test” (ISO 9972:2015, 2015). The fast and dependable detection of leaks is of critical importance, especially in the context of new constructions and the renovation of existing structures. Identifying and quantifying leaks using standard methods in conjunction with a blower door test, using tracer-gases (Ghazi & Marshall, 2014) for example, is a challenging, time-consuming process that is highly dependent on the experience of the respective energy consultant.

For this reason, various methods have been researched in recent years to overcome these weaknesses. Two prominent examples are the acoustic (Holstein, et al., 2020; Raman, Prakash, Ramachandran, Patel, & Chelliah, 2014) and thermographic (Mahmoodzadeh, Gretka, Wong, Froese, & Mukhopadhyaya, 2020) methods, both of which provide fast, simple and comprehensive detection and localisation of leaks in the building envelopes. While the acoustic beamforming method is based on a microphone array technology and assumes that sound primarily takes the same paths as air through the building envelope, the infrared camera can quickly identify problem areas through intelligent experimental setups such as lock-in thermography (Kölsch, Pernpeintner, Schiricke, & Lüpfert, 2023). Previous studies in both of this fields have demonstrated the potential of these technologies through measurements on existing buildings (Schiricke, Diel, & Kölsch, 2024) and on smaller façade elements (Feng, Shen, Shrestha, & Hun, 2024).

To the best of the authors' knowledge, no comprehensive laboratory studies have been conducted to date that employ either method in the context of leak detection in buildings. Such investigations have the advantage of further improving the reliability of leak detection by means of these measurement methods. Consequently, a laboratory test facility has been developed. The objective is to facilitate a comprehensive analysis of a multitude of leakages. A further area of interest is the variation and potential correlation in acoustic and thermal signatures according to the type and size of different leaks, as well as the conditions under which optimal localisation is possible.

2 METHODS

2.1 Test facility

The new test facility, designated ATLAS (Adaptable Testing Laboratory for Air Sealing), is located at the German Aerospace Center in Cologne, Germany. Figure 1 depicts the test facility, equipped with the essential measuring instruments.

The test facility is constructed on rollers, weighs approximately 500 kilograms and measures 2.0 meters in width, 2.5 meters in height and 3.0 meters in depth. An adapter plate is affixed to the posterior of the test facility, thereby enabling the attachment of a measuring fan. This fan is the Minneapolis DuctBlaster. The Minneapolis Micro Leakage Meter (MLM) system is connected to the adapter plate and the DuctBlaster via a hose system. The orifice within the MLM has a diameter of 4 mm, enabling the MLM to measure air volume flows in the range of 0.17 to 0.83 m^3/h at a pressure difference of 80 Pa. However, experimental examinations have demonstrated that even lower volume flows of approximately 0.1 m^3/h can be measured. The established blower door system characterizes the leaks by measuring the volume flow and will therefore help with the evaluation of the measurement results of the new measurement methods.

The test specimens can be attached to the front of the test facility using a quick-release mechanism. Two distinct sizes of test specimens can be clamped: the smaller specimens

measure 85 cm by 85 cm, while the larger specimens measure 170 cm by 170 cm. An acrylic glass plate (see Figure 1) serves as a reference plate for the measurement of the test facility's airtightness.

Figure 1: Test facility ATLAS equipped with its requisite measurement technology: Minneapolis DuctBlaster with Micro Leakage Meter (left), loudspeaker (inside), microphone array (right) and infrared camera (right)

In order to be able to measure the volume flow through emulated leakages of test specimens, the residual leakage of the test facility itself with an airtight reference plate as a specimen must first be measured. This value must then be subtracted from future measurements of other samples. The results of the residual leakage measurements are presented in Figure 2. In this experiment, the residual leakage was quantified three times for a chamber pressure of 50 Pa to 90 Pa in 10 Pa increments. Between each measurement series, the test specimen and door were removed and reinstalled to assess the reproducibility of the airtightness measurement. The average air flow of the linear regressions was 0.10 m^3/h for a pressure of 50 Pa, which corresponds to an n50 value of 0.0088. The maximum deviation of the regressions from the mean was 4.4 % for an overpressure of 50 Pa.

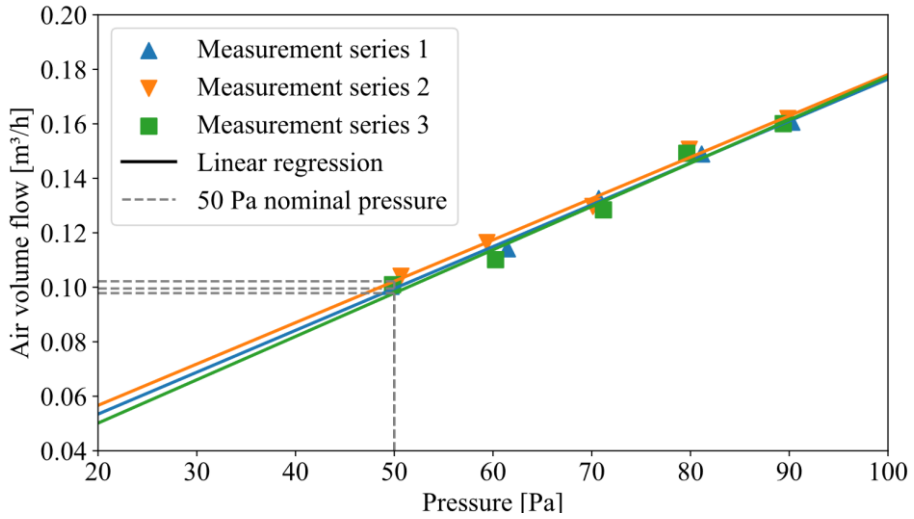

Figure 2: Reproducibility of residual leakage measurement at the ATLAS test facility using an acrylic reference plate as a test specimen

2.2 Acoustic leak detection

The localization of air leaks using an acoustic camera is based on the assumption that sound primarily follows the same path as air. In the measurements discussed here, the measurement setup for acoustic measurements consists of two components: the noise source, which is an omnidirectional transmitting loudspeaker and an amplifier connected to it, and the noise receiver, which is a microphone array (see Figure 1). Previous tests demonstrated that the positioning of the loudspeaker within the test facility had no impact on the measurement outcomes. For simplicity, the loudspeaker was therefore placed in the centre of the facility. The microphone array is situated at the height of the test specimen, at a distance of 1.5 meters. The camera utilized is the "Acoustic Camera Array Ring48 AC Pro" from gfai tech GmbH.

Acoustic camera measurement technology translates sound waves into a tangible representation by superimposing sound pressure level variations onto a visual image of the area of interest. Using beamforming, the camera accurately locates sound sources by considering the time it takes for the sound to reach each microphone. Advanced signal processing is essential for accurate measurement calculation and display. For a detailed description of this methodology, see the paper by Schiricke et al. (Schiricke, Diel, & Kölsch, 2024). In addition, the paper by Chiariotti et al. (Chiariotti, Martarelli, & Castellini, 2019) provides an in-depth explanation of beamforming.

2.3 Infrared leak detection

Leakages at building envelopes can be seen in infrared images, if there is airflow through the leak and the temperature of the leaking air and the surface surrounding the leak are not identical. Leaks can hence be emphasised by increasing the temperature difference, e.g. by blower heaters and by controlling pressure difference across the envelope using a blower door to increase the flowrate and control the direction of flow.

Leaks can be further separated from other structures in the image by active thermography. In that case, non-static blower operation is combined with image processing techniques. This can be as simple as taking differential images from before and after blower operation, as demonstrated by Kalamees (Kalamees, 2007). Time series analysis using physical models is performed in the BauTools Software distributed by BlowerDoor Gmbh and described by Feng et al. (Feng, Shen, Shrestha, & Hun, 2024). An approach, that will be investigated further in this test facility is lock-in thermography. There, the blower is activated periodically enabling the time series of the pixels to be analysed by Fourier transform at the excitation frequency, as described by Kölsch et al. (Kölsch, Pernpeintner, Schiricke, & Lüpfert, 2023).

However, for the first measurements presented here classical thermography is chosen. The camera is a Workswell Wiris Pro with an uncooled 640x514 pixel microbolometer sensor and 13 mm lens. The spectral range of the camera is 7.5-13.5 µm, the temperature sensitivity is specified to 30 mK. The time period for NUC-calibration was set to 3 minutes.

The camera is placed outside the test facility, compare Figure 1, and the test facility is operated at overpressure of 50 Pa creating airflow towards the camera. The camera is placed at distances of approximately 150 cm, 250 cm, and 500 cm from the test section, perpendicular to the test section, in one measurement at distance 150 cm, but at a 45° angle to the side. Fan heaters within the test facility heat the interior to 27°-28 °C, which is 6 K-7 K above the temperature of the laboratory at 21 °C. For the radiometric evaluation, emittance was set to 91% (Stephan,

et al., 2019), reflected temperature, temperature of atmosphere, and temperature of the lens to 21°C and relative humidity to 40%.

3 RESULTS

3.1 Acoustic measurements

The results of three smaller measurement campaigns conducted with the acoustic setup on the ATLAS are presented below.

In the first series of measurements, the capacity of the acoustic system to identify the location of leaks at varying measuring distances was examined. To this end, a hole with a diameter of 3.3 mm was drilled into a 12 mm thick medium-density fibreboard. Four distinct measurement distances were examined, maintaining consistent noise source settings. The distances investigated were 0.5 m, 1.5 m (the standard configuration at the test facility), 2.5 m, and 5.0 m. Figure 3 depicts the acoustic images, which demonstrate that the hole could be localized at each distance. Nevertheless, the measured sound pressure level exhibited a decreasing trend with increasing distance of the array from the test specimen. In the 10 kHz third octave band, the sound pressure level at the hole was 16.6 dB for a measurement distance of 0.5 m and 5.9 dB at a distance of 5 m.

As part of the second series of measurements, the impact of varying hole sizes was examined. For this purpose, holes with diameters of 3.3 mm, 4.2 mm, 5.0 mm, 5.5 mm, and 6.0 mm were drilled into a particle. The experimental configuration, including the array spacing and output signal of the loudspeaker, remained constant throughout the experiments. Figure 4 illustrates the frequency spectra of the individual holes. Up to a frequency of 6 kHz, all holes display a highly similar acoustic signature. At higher frequencies, the sound pressure level curves continue to be similar in their monotonic behaviour, but there are noticeable differences in the maximum sound pressure level. The largest difference between the 3.3 mm and 6.0 mm holes is at a frequency of 9.84 kHz and is 7.64 dB. In addition, the sound pressure level for the largest hole is on average 5.37 dB higher in the range between 8 kHz and 16 kHz. All comparative data between each hole is shown in Table 1 below.

In the final series of measurements, the capacity of the acoustic measurement system to differentiate between holes in close proximity was examined. The identical configuration was utilized as in the preceding series. Three distinct distances were evaluated, comprising two 3.3 mm holes situated 30 mm, 40 mm, and 50 mm from the centre of the hole. The acoustic images are illustrated in Figure 5. In the case of the smallest hole spacing, the camera was unable to differentiate between the two holes at any frequency range. This was also the case for a hole spacing of 40 mm. However, the acoustic image displays a less punctual and more elongated local sound pressure level peak compared to the previous measurement. With the largest hole spacing, on the other hand, both sources could be easily differentiated. In this case, the ratio of measuring distance to hole spacing is 30.

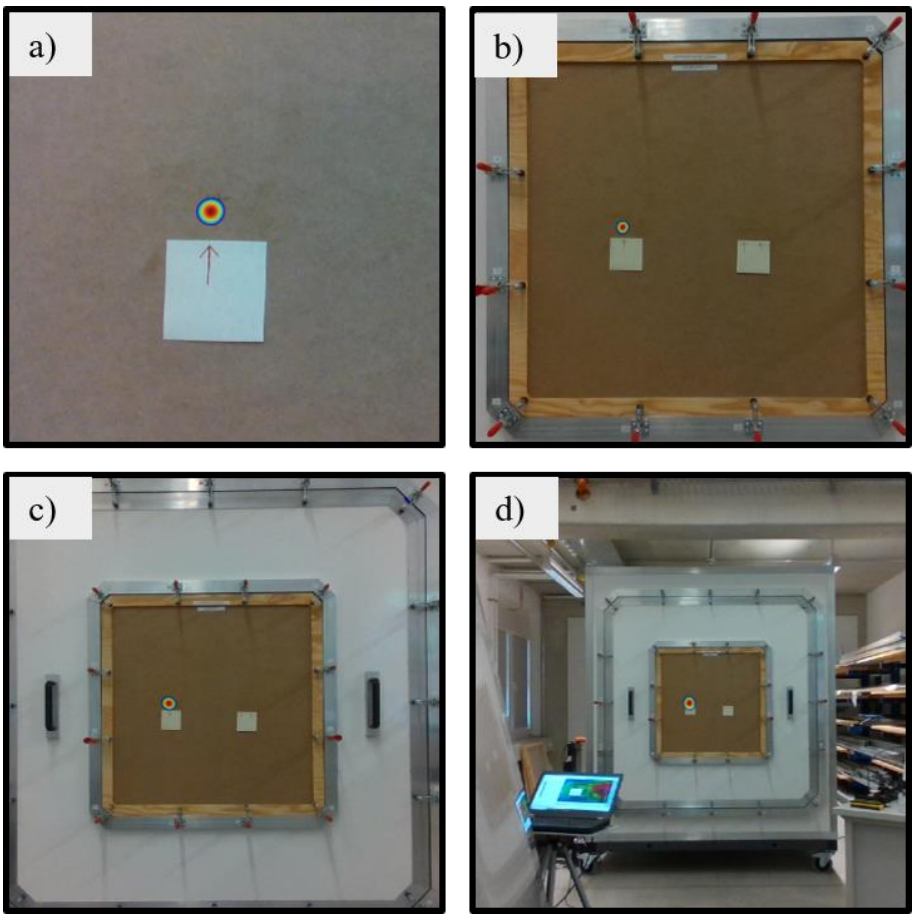

Figure 3: Recording of the acoustic camera of a 3.3 mm hole at a measuring distance of: a) 0.5 m, b) 1.5 m, c) 2.5 m, d) 5.0 m

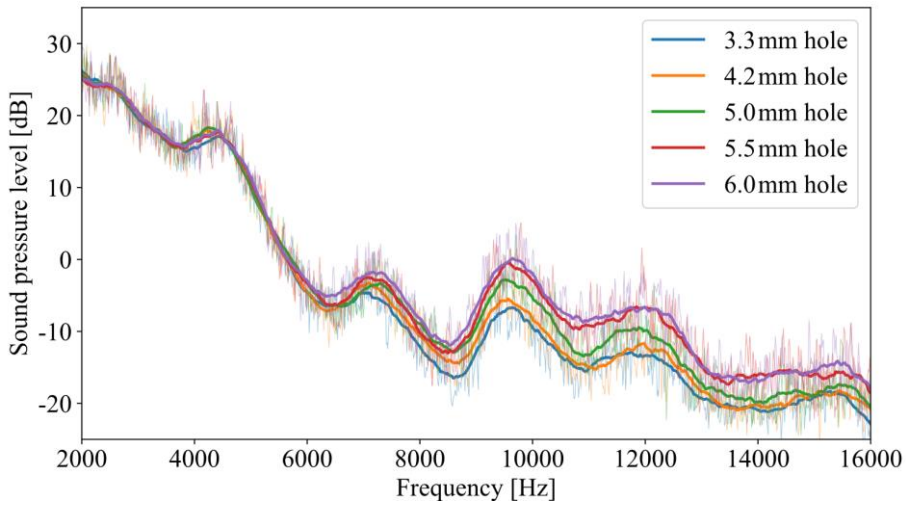

Figure 4: Moving average smoothed sound pressure level curve for five different hole sizes

Table 1: Comparison between measured sound pressure levels of different hole sizes

Hole size in mm	**3.3**	**4.2**	**5.0**	**5.5**	**6.0**
a = Hole area in $10^{-6}\times m^2$	8.55	13.85	19.63	23.76	28.27
p_m = Mean sound pressure level between 8 kHz to 16 kHz in dB	-15.78	-14.95	-13.24	-11.04	-10.42
p_m/a in $dB/m^2\times10^5$	-18.45	-10.79	-6.74	-4.65	-3.68

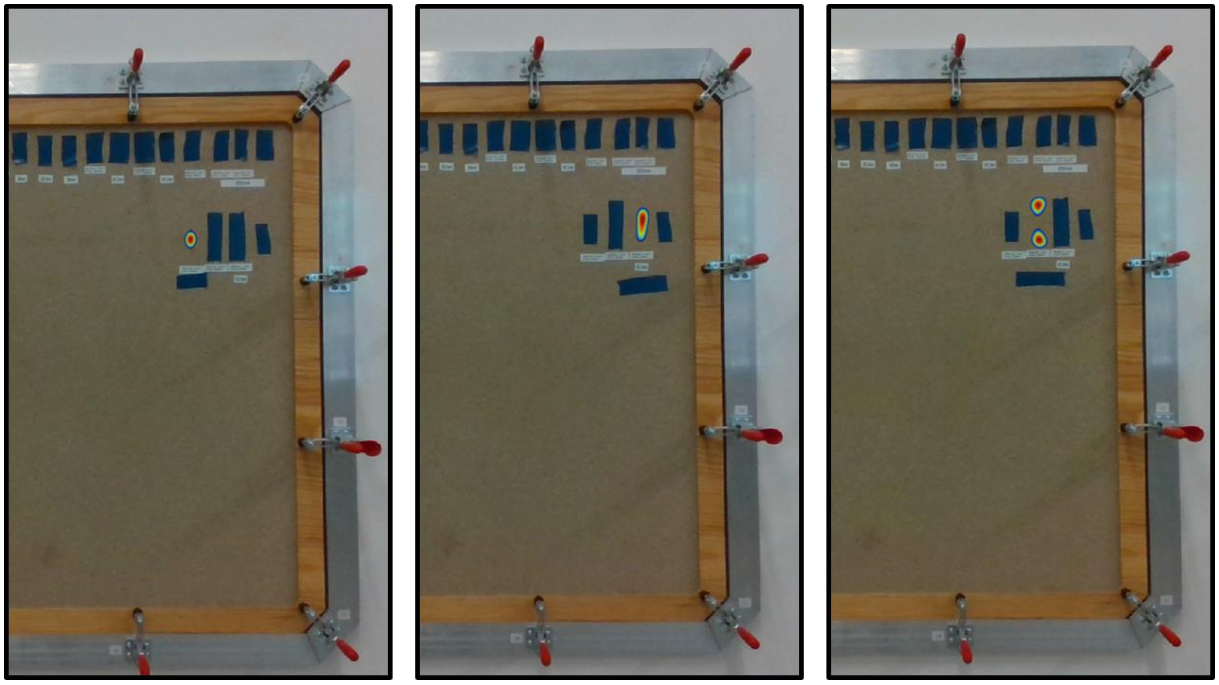

Figure 5: Acoustic camera recordings of two 3.3 mm holes at a distance of 30 mm (left), 40 mm (centre) and 50 mm (right) from each other

3.2 Infrared measurements

For the infrared measurements, a number of holes in the specimen (thickness 13 mm) were used ranging in diameter from 6 mm to 2 mm, compare Figure 6. This was the same test specimen used in the second and third series of acoustic tests. The distance of the holes (some covered by tape) is 40 mm. This compares to the pixel-resolution of the camera in the plane of the specimen of 2.0 mm at 150 cm, 3.3 mm at 250 cm and 6.5 mm at 500 cm camera distance.

Figure 8 b) to e) shows the result of four measurements at different distances and angles. In order to create comparable colour settings for all images in Figure 8 b) to e), the colour settings are adjusted to show identical range of 3 K, with the measured temperature of the specimen at a fixed colour, compare Figure 8 a). The images taken at 250 cm and 500 cm are cropped to show the same image section as the image taken at 150 cm camera distance.

First, images Figure 8 b) to e) are compared visually: The two small holes at the right cannot be separated in any image and appear in all images as a single leak. All other leaks can be separated. With larger camera distance, the temperature signal is reduced. A pixel increasingly images not only the hole but also the surrounding specimen. This is also visible in the profiles plotted in Figure 7. The larger the camera distance, the lower the measured peak value, and the wider the peak. For temperature measurements, it is typically recommended, that structures should be at least 3 pixels wide. As we are only interested in the location of the leak a reduction in signal is acceptable.

It is noteworthy, that in the measurement at 45° and 150 cm, compare Figure 8e), the signal is also significantly reduced - compared to the measurement at normal incidence and at identical distance, compare Figure 8b). At 45° the camera only visualises the internal walls close to the surface, where the temperature difference to the ambient is smaller than further inside.

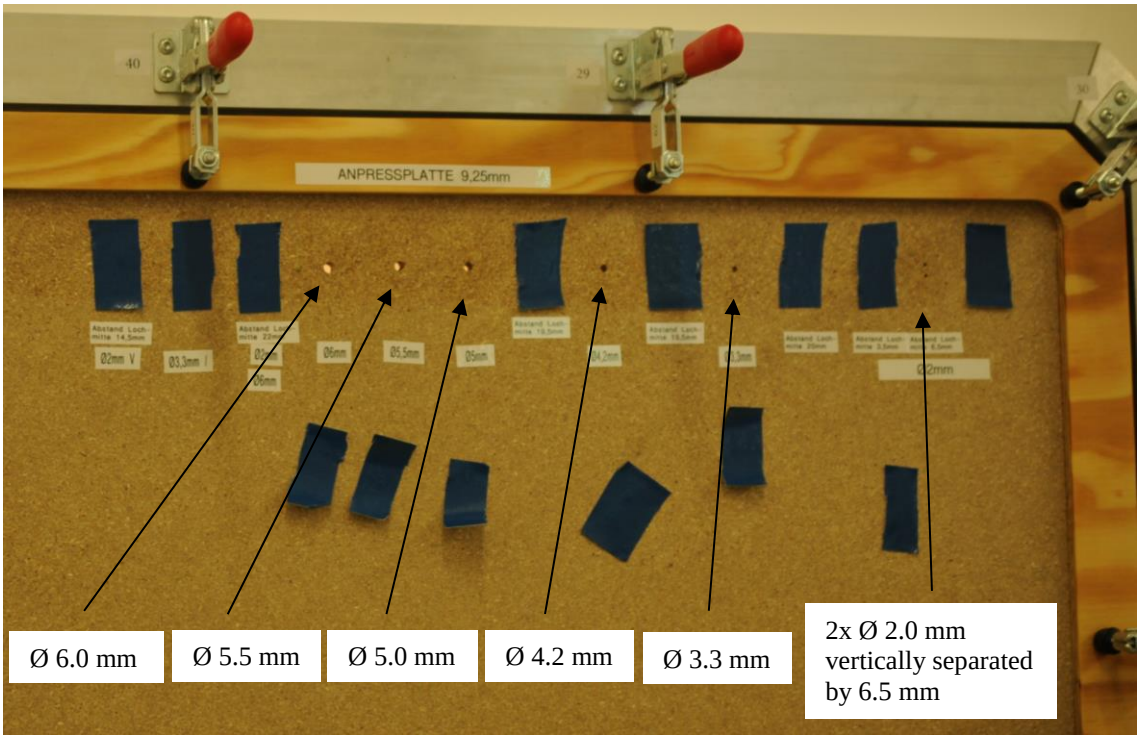

Figure 6: Specimen for infrared measurements, additional holes are covered by tape

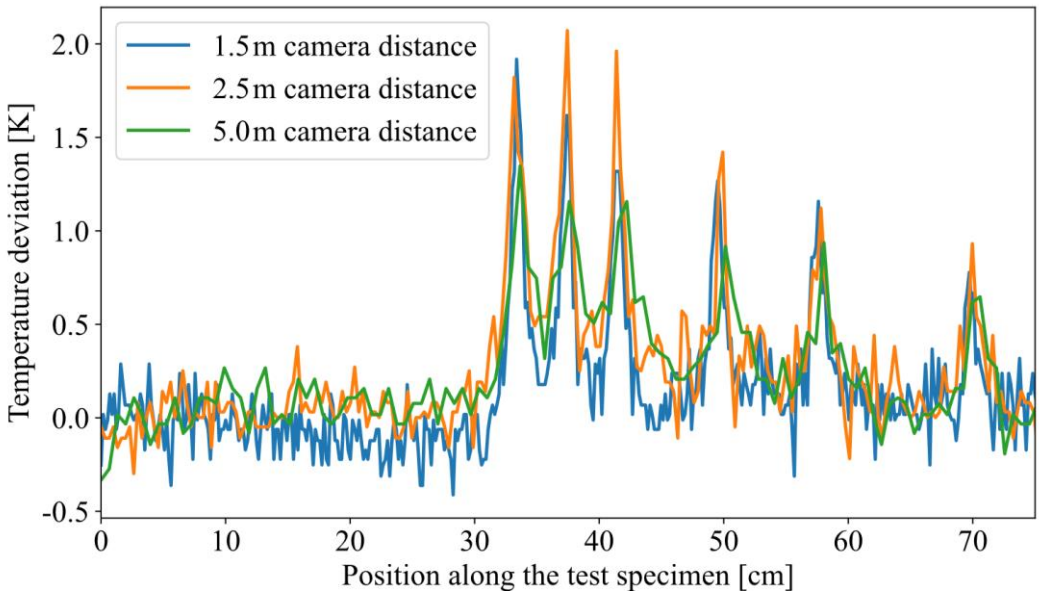

Figure 7: Temperature profile of specimen for three camera distances

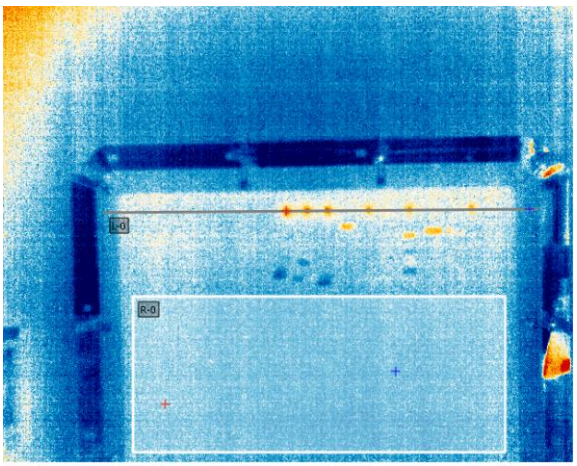

T_{max} = mean(T_{R-0}) + 2 K

T_{min} = mean(T_{R-0}) – 1 K

a) Temperature scales are adjusted for all images a) to e) from offsets by –1 K for minimum temperature (blue) and by +2 K for maximum temperature (red) from mean temperature of the unobstructed board (area R-0 in a); line L-0 is defined for evaluation of temperature profile containing the leakage positions

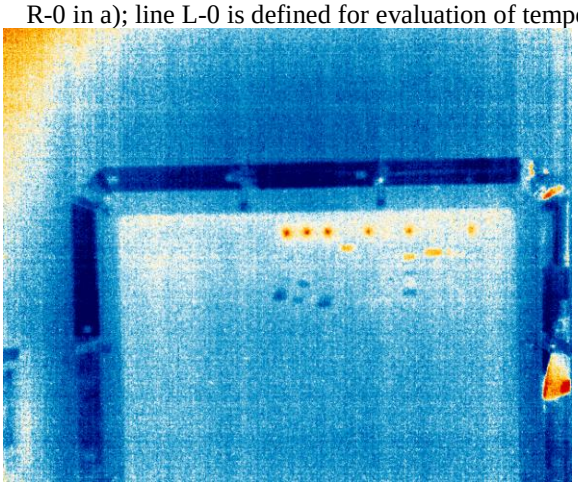

b) Camera distance 150 cm, full image, pixel resolution 2.0 mm

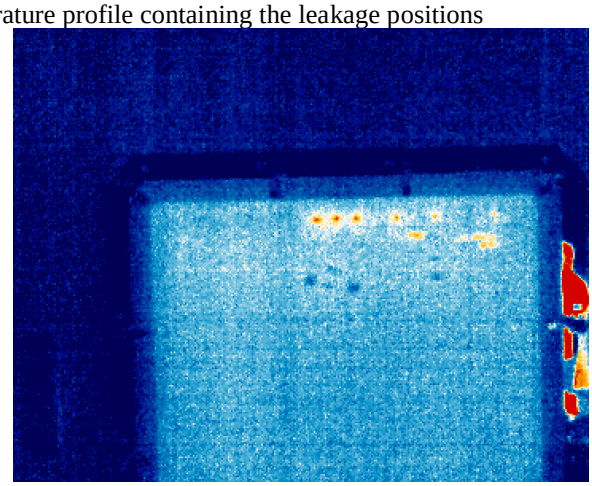

c) Camera distance, 250 cm, image cropped, pixel resolution 3.3 mm

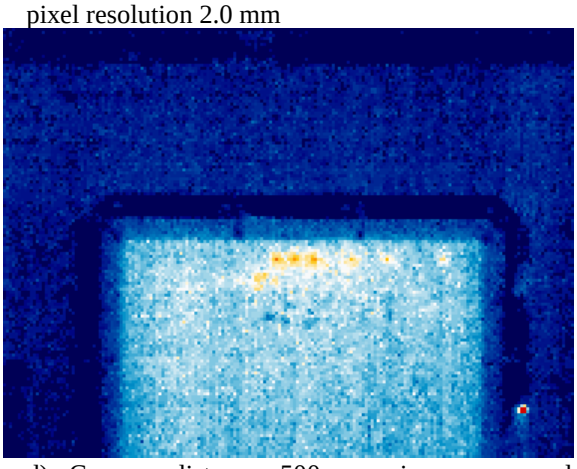

d) Camera distance 500 cm, image cropped, pixel resolution 6.5 mm

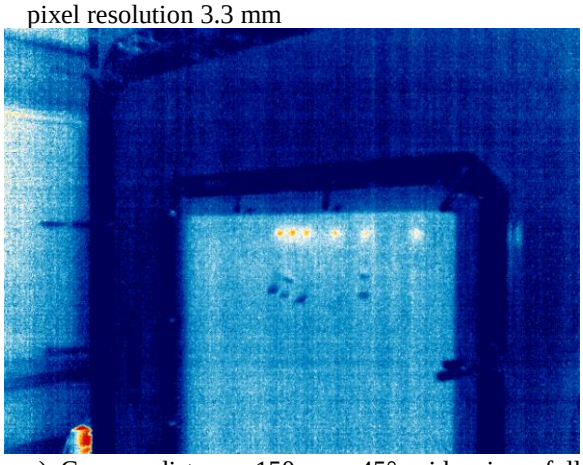

e) Camera distance 150 cm, 45°- side view, full image, pixel resolution 2.0 mm

Figure 8: Infrared images of the test specimen at different distances and angles

4 CONCLUSIONS & OUTLOOK

The measurements demonstrate that the test facility offers a more controllable environment than field measurements, resulting in higher reproducibility and comparability of the measurements. Furthermore, the leakages can be measured individually, which significantly simplifies the characterisation of a single leakage. This can be observed in the air volume flow measured with the MLM, the acoustic signature and the thermographic image.

The acoustic measurements showed that small leaks can be localised at different measuring distances. Furthermore, a first correlation between measuring distance and hole spacing for the ability to distinguish holes from each other could be determined. Whether this is a constant or variable value needs to be clarified in further experiments. In addition, measurements on leaks of different sizes showed that the same leak types have similar spectral characteristics, and that the size of the sound pressure level peaks may allow conclusions to be drawn about the size of the leaks. In the context of future investigations, it will be of great relevance to ascertain whether this behaviour is also observed in other leakage types. In particular, it will be beneficial to determine the role of different spectral ranges on the ability of locating leaks, and whether an automated evaluation can be realised with a sufficiently large data basis.

The first IR-images were taken at various distances and angles showing that leaks smaller than the pixel resolution can be detected with reduced signal, as the traditional limits for temperature measurements do not apply. In addition, a reduction in signal was found at lower angles of incidence, reflecting the fact that the visible depth increases at angles closer to normal, where larger temperature differences can be observed.

In future experiments, more complex leakages will be investigated. Parameters such as the leakage path, the material through which the air passes as well as the entry and exit paths of air/sound (e.g. simple crack or socket) will be of special interest.

5 ACKNOWLEDGEMENTS

This work is part of the ongoing joint research project “Development of a combined method of acoustics and infrared thermography for quantitative evaluation of the airtightness of building envelopes and locating leaks (Q-Leak)”, conducted by the German Aerospace Center (DLR) with its project partners Gesellschaft zur Förderung angewandter Informatik e.V. (GFaI), SONOTEC GmbH, Ecoworks GmbH, BlowerDoor GmbH, alstria office REIT- AG. This project is funded by the German Federal Ministry for Economic Affairs and Climate Action (BMWK) under the grant number 03EN1079A. The authors would also like to thank Imke Grzemba and Karl Woitke from “R316 KontruktionsWerkstatt” for building the test facility.

6 REFERENCES

Chiariotti, P., Martarelli, M., & Castellini, P. (2019). Acoustic beamforming for noise source localization--Reviews, methodology and applications. *Mechanical Systems and Signal Processing*(120), 422-448. doi:https://doi.org/10.1016/j.ymssp.2018.09.019

Feng, T., Shen, Z., Shrestha, S. S., & Hun, D. E. (2024). A novel transient infrared imaging method for non-intrusive, low-cost, fast, and accurate air leakage detection in building envelopes. *Journal of Building Engineering*. doi:https://doi.org/10.1016/j.jobe.2024.109699

Ghazi, C., & Marshall, J. (2014). A CO2 tracer-gas method for local air leakage detection and characterization. *Flow Measurement and Instrumentation, 38*, 72-81. doi:https://doi.org/10.1016/j.flowmeasinst.2014.05.015

Holstein, P., Bader, N., Moeck, S., Münch, H.-J., Döbler, D., & Jahnke, A. (2020). Akustische Verfahren zur Ermittlung der Luftdichtheit von Bestandsgebäuden. *Denkmal und Energie 2020: Energieeffizienz, Nachhaltigkeit und Nutzerkomfort* (pp. 111-123). Springer. doi:https://doi.org/10.1007/978-3-658-28753-5_8

ISO 9972:2015. (2015). *Thermal Performance of Buildings—Determination of Air Permeability of Buildings—Fan Pressurization Method*. International Organization for Standardization: Geneva, Switzerland.

Jokisalo, J., Kurnitski, J., Korpi, M., Kalamees, T., & Vinha, J. (2009). Building leakage, infiltration, and energy performance analyses for Finnish detached houses. *Building and Environment, 44*(2), 377-387. doi:https://doi.org/10.1016/j.buildenv.2008.03.014

Kalamees, T. (2007). Air tightness and air leakages of new lightweight single-family detached houses in Estonia. *Building and environment, 42*(6), 2369-2377. doi:https://doi.org/10.1016/j.buildenv.2006.06.001

Kölsch, B., Pernpeintner, J., Schiricke, B., & Lüpfert, E. (2023). Air leakage detection in building façades by combining lock-in thermography with blower excitation. *International Journal of Ventilation, 22*(4), 357-365. doi:https://doi.org/10.1080/14733315.2023.2198791

Mahmoodzadeh, M., Gretka, V., Wong, S., Froese, T., & Mukhopadhyaya, P. (2020). Evaluating patterns of building envelope air leakage with infrared thermography. *Energies, 13*(14). doi:https://doi.org/10.3390/en13143545

Raman, G., Prakash, M., Ramachandran, R. C., Patel, H., & Chelliah, K. (2014). Remote detection of building air infiltration using a compact microphone array and advanced beamforming methods. *Berlin Beamforming Conference*, (pp. 1-10).

Sawyer, K. (2014). Windows and Building Envelope Research and Development: Roadmap for Emerging Technologies. *US Department of Energy: Washington, DC, USA*.

Schiricke, B., Diel, M., & Kölsch, B. (2024). Field Testing of an Acoustic Method for Locating Air Leakages in Building Envelopes. *Buildings, 14*(4). doi:https://doi.org/10.3390/buildings14041159

Stephan, P., Kabelac, S., Kind, M., Mewes, D., Schaber, K., & Wetzel, T. (2019). *VDI-Wärmeatlas: Fachlicher Träger VDI-Gesellschaft Verfahrenstechnik und Chemieingenieurwesen.* Springer-Verlag.